

Progress in high-voltage MgMn_2O_4 oxyspinel as a cathode material in Mg batteries

Alexandra Michail^a, Begoña Silvan Uriarte^a and Nuria Tapia-Ruiz^{a,*}

^a Department of Chemistry, Lancaster University, Lancaster, LA1 4YB, United Kingdom.

* Corresponding author

Abstract

Rechargeable magnesium batteries (RMBs) are a promising post-lithium battery technology that benefits from the use of a Mg metal anode, which provides a high volumetric capacity (3833 mAh cm^{-3}), low reduction potential and dendrite-free deposition. In parallel to the development of novel electrolytes compatible with Mg, the future realisation of RMBs demands cathode materials with high energy densities and suitable Mg intercalation kinetics. In this mini-review, the focus will be laid on the high-voltage intercalation MgMn_2O_4 oxyspinel cathode (and substituted derivatives). We aim at providing an updated understanding of the reaction mechanisms occurring during (de)magnesiumation of MgMn_2O_4 , and the role of Mg/Mn anti-site defects in its electrochemical behaviour. We then critically evaluate the performance of MgMn_2O_4 in organic and aqueous-based electrolytes, highlighting their merits and challenges, and provide an overview of the most recent developments to improving battery performance. Finally, we will highlight key areas that require further attention to provide an understanding of their charge storage behaviour.

Introduction

Uncertainties regarding the future of lithium-ion batteries (LIBs) due to the projected increased demand for lithium-based electrodes in the mobility and renewable energy sectors focus on the sustainability and cost of lithium.¹ Consequently, considerable efforts have been devoted to exploring novel rechargeable batteries which may complement LIBs based on sustainable, low-cost and abundant metals. Among these, rechargeable magnesium batteries (RMBs) are particularly promising since they can theoretically achieve a volumetric capacity of 3883 mAh cm^{-3} (*cf.* 2044 mAh cm^{-3} for Li) and a gravimetric capacity of 2205 mAh g^{-1} (*cf.* 3862 mAh g^{-1} for Li), with a low redox potential of $E_{\text{Mg}^{2+}/\text{Mg}} = -2.37 \text{ V}$ vs. standard hydrogen electrode (SHE) when using Mg metal anodes.² The absence of dendritic growth upon Mg plating/stripping in adequate electrolyte solutions³ provides RMBs with excellent safety features and prospects for long cycling life. However, the use of Mg metal as an anode leads to the formation of an insulating passivation surface layer on the metal when in contact with reducible species such as water, oxygen, and various organic impurities.⁴ Therefore, suitable electrolyte solutions that allow a passivation-free Mg surface are required to enable Mg stripping/plating while showing

high ionic conductivity and high anodic stability. We refer the readers to references ^{5,6} for further details on electrolyte development.

From the positive electrode (cathode) materials perspective, an additional challenge occurs when using divalent Mg^{2+} ions as the charge carriers. The high charge/radius ratio of Mg^{2+} ions causes a strong electrostatic interaction with ions in the cathode host which directly influences the electronic structure and limits the diffusion of the ions within the cathode lattice, resulting in large voltage hysteresis.⁷

Oxyspinel-structured cathode materials for RMBs

In the search for materials that deliver higher voltages and capacities, a variety of cathode materials including transition metal oxides, sulphides, organic compounds and metallic particles have been explored for Mg intercalation.⁸⁻¹⁰ These can be classified into intercalation and conversion compounds, being the former class, in turn, divided into materials with 3D (e.g. Chevrel phases and spinel), 2D (e.g. TiS_2 , $\alpha-V_2O_5$ and $\alpha-MoO_3$) and 1D (olivine-type materials) diffusion pathways and open framework (Prussian blue analogues) for Mg diffusion. A summary table indicating selected performance metrics of the most relevant intercalation cathode materials is shown in Table 1.¹⁰

Table 1. Summary of selected performance metrics of most relevant 3D, 2D, 1D and open framework cathode materials for RMBs. Adapted from reference 10.

Intercalation type	Structure type	Material	Diffusivity (meV)	Potential (V)	Capacity (mAh g ⁻¹)
3D	Chevrel phase	Mo_6S_8	360	0.99, 1-1.3	120
	Spinel	Mn_2O_4	~650-850	2.86, 2.9	270
2D	Layered sulfide	TiS_2	1160	~1	115
	Layered oxide	$\alpha-V_2O_5$	975-1120	2.21, 2.35	150
1D	Olivine	$FePO_4$	580-1025	~2	12
Open framework	Prussian blue analogues	Nickel hexacyanoferrate	-	2.9	80

Cathode materials with 3D channels for Mg diffusion are in principle one of the most popular materials' choices since these shall facilitate Mg ion mobility. Among these, Chevrel phases of the Mo_6T_8 family (T = S, Se, or their combination) have demonstrated specific capacities ~ 130 mAh g⁻¹ with an average discharge voltage of ca. 1.2 V vs. Mg^{2+}/Mg , which lead to low theoretical energy densities (ca. 135 WhK g⁻¹), which are considered low for some

applications.¹¹ On the other hand, MgMn_2O_4 oxyspinels materials, with frustrated tetrahedral coordination of Mg, robust structure and switchable redox properties show promising performance metrics, with theoretically higher capacities that can be delivered at a higher voltage, thus with higher energy densities than the Chevrel phases.^{12,13} Okamoto et al. studied the feasibility of MgB_2O_4 spinels (B= Mn, Co, Fe and Cr) as RMB cathode materials.¹⁴ These were tested in beaker cells using $\text{Mg}(\text{TFSA})_2$ in ionic liquid electrolyte at 150 °C. The authors showed that Mg insertion to form a fully magnesiated compound of the $\text{Mg}_2\text{B}_2\text{O}_4$ - type was possible when B= Co or Mn through the reduction reaction of B^{3+} ions to B^{2+} ions at 2.9 and 2.3 V vs. Mg^{2+}/Mg , respectively. Mg insertion was reported to be possible due to the stability of the MgO and BO rocksalt phases formed in the process. Mg extraction could be realized from the Mn-based spinel compound through the $\text{Mn}^{3+}/\text{Mn}^{4+}$ redox couple at 3.4 V Mg^{2+}/Mg . Further ab-initio calculations corroborated these results, showing that the thermodynamic stabilities of the charged and discharged states in Mn_2O_4 were most promising compared to other spinel materials where B= Ti, V, Cr, Mn, Fe, Co and Ni.¹³ The authors suggested that improved thermodynamic stabilities could lead to improved cycle life as well as better synthesizability. This same report suggested the Mn-based spinel structure to be the best candidate when balancing different properties such as specific energy, voltage, phase stability, thermal stability and cation mobility. Given the ability of MgMn_2O_4 to reversibly insert and extract Mg^{2+} ions together with its low-cost, suitable average voltage and superior theoretical specific capacity (540 mAh g^{-1})^{15,(*)} the Mn-based spinel is accountable for most of the published reports to date.

In this mini-review, we provide a critical overview of the recent progress and current challenges related to the MgMn_2O_4 oxyspinel. Particular emphasis is placed on providing an updated understanding of the reaction mechanism of Mg (de)insertion in the tetragonal and cubic MgMn_2O_4 polymorphs and the formation of Mg/Mn anti-site defects and their relation to electrochemical behaviour. We also examine the performance of MgMn_2O_4 when coupled with organic and aqueous electrolytes and provide a review of different optimisation strategies to advance toward high-performance RMB batteries. Last, we summarise some remaining challenges ~~key areas~~ that still require further investigation for the realization of these materials in RMBs.

MgMn₂O₄ Polymorphs and Inversion Degree

Oxyspinels, with the general formula AB_2O_4 , crystallise in the cubic space group ($Fd\bar{3}m$), where the divalent cations, A, occupy the tetrahedral sites (8a) and the trivalent cations, B, occupy the octahedral sites (16d).¹⁶ In the case of MgMn_2O_4 , the presence of Jahn-Teller active Mn^{3+} ions results in a lower tetragonal symmetry with space group ($I41/amd$).¹⁷ Unlike

other spinels, e.g. ZnMn_2O_4 and CdMn_2O_4 , MgMn_2O_4 shows a tendency for Mg/Mn anti-site disorder, also known as inversion (i), which is triggered by the disproportionation of Mn^{3+} ions (i.e. $2 \text{Mn}_{\text{oct}}^{3+} \rightarrow \text{Mn}_{\text{tet}}^{2+} + \text{Mn}_{\text{oct}}^{4+}$) whereby isovalent Mn^{2+} ions can substitute for Mg^{2+} ions.¹⁸ In an inverted spinel, Mg^{2+} ions are found in both 8a and 16d tetrahedral and octahedral sites, Mn^{3+} ions and Mn^{4+} are located in 16d octahedral sites and Mn^{2+} ions are found in 8d tetrahedral sites.^{19,20} High temperatures increase the inversion degree in the MgMn_2O_4 tetragonal phase leading to the formation of the cubic MgMn_2O_4 phase.^{20,21} Nevertheless, the inversion reaction is reversible when cooling down to ambient temperature.²¹ First-principle calculations and percolation theory showed that Mg/Mn anti-site disorder has a strong interdependence on Mg mobility across different migration trajectories in the MgMn_2O_4 tetragonal polymorph, which percolates Mg up to $i \approx 55\%$ (**Figure 1a**).^{22,(*)} The same authors reported that low inversion degrees ($i < 0.4$) can significantly reduce the extractable capacity in MgMn_2O_4 , with an estimated 15% decrease in capacity with every 10% increase in inversion. On the other hand, Kwon et al. demonstrated experimentally that reducing Mg/Mn the inversion degree in pristine MgCrMnO_4 from $i = 0.16$ to 0.1 by re-annealing the powders at 350 °C, led to a remarkable decrease in the electrode polarisation and increased the capacity at the potential of ~ 0.4 V (vs. carbon) when the electrode was cycled at 95 °C.^{23,(*)}

The cubic phase has been reported to exist as a single-phase at extreme synthesis conditions (e.g. at high-temperatures (> 950 °C),^{20,24} high-pressure (> 15.6 GPa),²⁵ when synthesised using pulsed laser deposition (PLD))²⁶ and more recently, via an alcohol reduction process (**Figure 1b**).^{27,(*)} Feng et al. suggested a lower Mg^{2+} diffusion barrier in the cubic phase with respect to the tetragonal phase due to a high level of site mixing and percolation pathways in epitaxially stabilised thin films, showing charge capacity values of ca. 250 mAh g^{-1} .²⁶ However, when the cubic spinel powders are electrochemically tested (i.e. 5 nm nanoparticles) only very modest capacity values of ca. 60 mAh g^{-1} were achieved, being its performance only improved when used in graphene composites, exhibiting a specific capacity of 230 mAh g^{-1} .²⁷ Therefore, other factors including preferred orientation must be accounted for the higher Mg^{2+} diffusivity in the cubic polymorph.

A third MgMn_2O_4 polymorph that crystallises in the orthorhombic $Pmab$ space group (similar to that of Mn_3O_4)²⁸ was reported by Malavasi *et al.* upon subjecting the tetragonal phase to pressures around 14.4 GPa.²⁹ Two inverted tetragonal phases with $i = 0.2$ and 0.4 were used for the study, showing that the transition pressure was reduced by 1GPa in the more inverted sample. Later, first-principles evaluations have confirmed the $Pmab$ phase to be the most stable at high pressure and estimated the tetragonal to orthorhombic transition to occur at ~ 11.1 GPa³⁰ although they predicted very high migration barriers for this post-spinel. To date,

however, there is no experimental evidence of the electrochemical performance of this post-spinel as an RMBs cathode material to corroborate this.

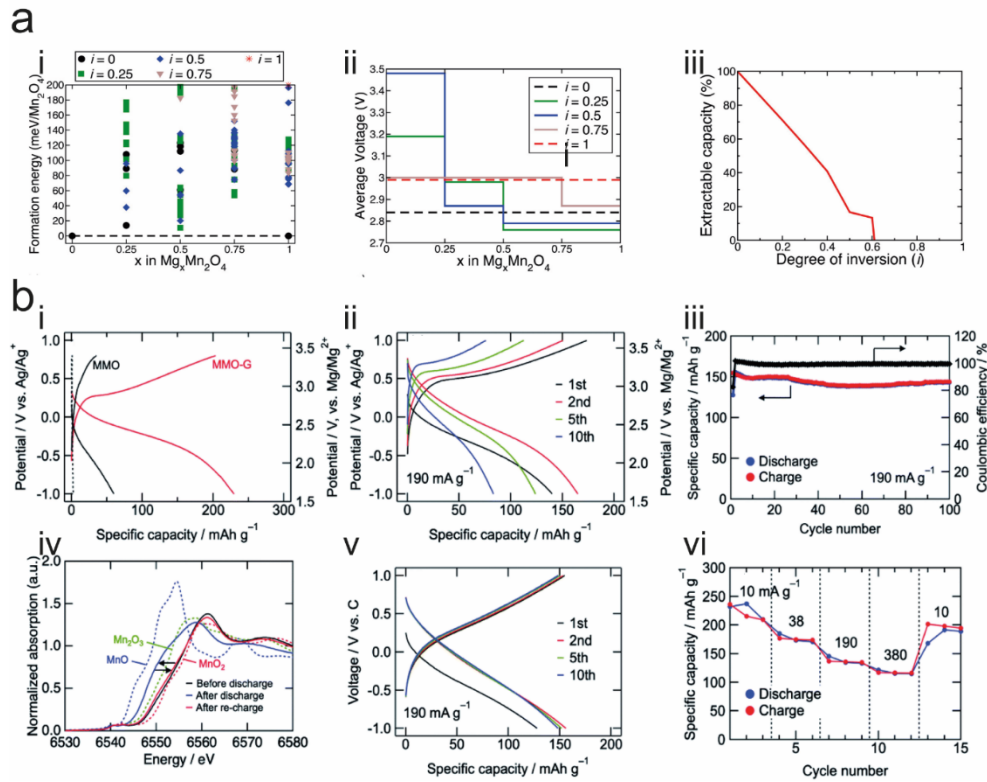
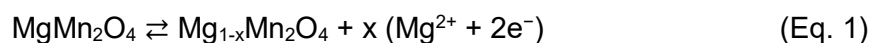
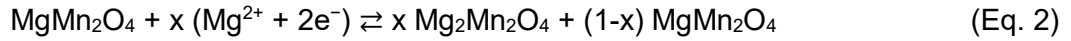


Figure 1 (a) (i) Ground state hull (or 0 K phase diagram) of the $Mg_xMn_2O_4$ system, with the zero of the formation energy referenced to the noninverted ($i = 0$) magnesiated ($MgMn_2O_4$) and empty (Mn_2O_4) spinel configurations. (ii) Average voltage curves under i in $Mg_xMn_2O_4$, obtained using the lowest formation energy structures at each i across Mg concentrations. (iii) Percentage of the theoretical capacity that can be reversibly extracted is plotted as a function of inversion in stoichiometric $MgMn_2O_4$.^{22,(*)} (Reproduced from ref. 22 with permission from American Chemical Society, Copyright 2017) (b) (i) Voltage curves of $MgMn_2O_4$ (MMO) and composite of $MgMn_2O_4$ with graphene (MMO–G) cathodes, (ii) Mn K-edge XANES spectra of MMO–G cathodes. (iii) Voltage curves of MMO–G cathode at 190 $mA\ g^{-1}$ using a 3-electrode cell or (iv) a coin-type cell. (v) Cyclability and (vi) rate-capability tests of MMO–G cathode using a coin-type cell.^{27,(*)} (Reproduced from ref. 27 with permission from The Royal Society of Chemistry, Copyright 2019)

MgMn₂O₄ charge compensation mechanism

Tetragonal $MgMn_2O_4$ can exhibit a theoretical capacity of 540 $mAh\ g^{-1}$ when using both Mn^{3+}/Mn^{4+} and Mn^{3+}/Mn^{2+} redox couples. The Mg insertion/extraction reactions occurring in $MgMn_2O_4$ can be described as follows:





The extraction of Mg^{2+} ions from MgMn_2O_4 has a lower energy barrier compared to their insertion.^{31,(*)} However, the lack of suitable high-voltage electrolytes with high anodic stability leads to parasitic electrolyte reactions that compete against Mg extraction processes. Likewise, the absence of consensus in the literature with regards to the use of a standard electrolytic solution and testing temperatures explain the diverse values reported in the literature for Mg extracted from the spinel host in the charging process, which go up to $x = \sim 0.4$ Mg per formula unit.³² Mg extraction in MgMn_2O_4 occurs at ca. 3.5 V vs Mg^{2+}/Mg through a solid-solution reaction followed by a biphasic reaction of the tetragonal spinel and a Mg-defect cubic spinel. On the other hand, Truong et al. studied the charge mechanism described in Eq. 1 on the cubic MgMn_2O_4 polymorph using spherical aberration-corrected scanning transmission electron microscopy (STEM).³³ They observed a structural transition from cubic to tetragonal spinel which they attributed to charge ordering of Mn^{3+} and Mn^{4+} due to a cooperative Jahn-Teller effect (**Figure 2a**).^{15,(*)} They also suggested the activation of the $\text{Mn}^{4+}/\text{Mn}^{5+}$ redox couple during deintercalation although they acknowledged that further work was required to substantiate this conjecture.

Conversely, Mg insertion into the octahedral 16c vacant sites in the MgMn_2O_4 phase (Eq. 2), occurs at a potential of ca. 2.3 V vs. Mg^{2+}/Mg via an *insertion and push-out process*, leading to the formation of a $\text{Mg}_2\text{Mn}_2\text{O}_4$ rocksalt structure^{14,34,(**)} as observed in LiMn_2O_4 .³⁵ However, $\text{Mg}_2\text{Mn}_2\text{O}_4$ formation was only explained with electrochemical data and qualitative changes in the X-ray diffraction and X-ray absorption near-edge spectroscopy data and thus, the level of magnesiation in MgMn_2O_4 (as well as the limit of reversibility in this reaction) remains unclear.¹⁴ Using STEM it was observed that the rocksalt phase grows on the surface of the MgMn_2O_4 spinel (*Fd-3m* space group), while the bulk of the particles retain the spinel structure even after 50 cycles (**Figure 2b**).³³ The rocksalt phase is responsible for an increase in the charge-transfer resistance with respect to the pristine electrode caused by a lattice mismatch between the MgO and MnO discharge phases which results in a large overpotential upon cycling and capacity fading.³³ This explains the improvement in cycling stability observed by Medina et al. when using concentration cells with MgMn_2O_4 (*I41/amd*) and $\text{Mg}_{0.3}\text{Mn}_2\text{O}_4$ electrodes to suppress the formation of the fully discharged reaction products.³⁶ Subsequently, later works have focussed on improving the reversibility of the inverse rocksalt-spinel reaction. For example, by replacing Mg ions with Zn ions which have a tendency to occupy the tetrahedral sites.^{34,(**)}

More recently, Tuerxun et al. showed that the Mg^{2+} insertion mechanism proceeds through three different stages (two solid-solution processes followed by a spinel-rocksalt coexistence

process) (**Figure 2c**), and not through a simple two-phase reaction mechanism between the spinel phase and rocksalt phases using a combination of techniques including electrochemical measurements and ex-situ synchrotron X-ray absorption spectroscopy (XAS) and diffraction (XRD).³⁷ However, the studies were performed on a pristine material with formula $\text{Mg}_{1.04}\text{Mn}_2\text{O}_4$ which consisted of a mixture of spinel cathode phase (86%) with *I41/amd* space group and 14% rocksalt phase with *Fm-3m* space group. It is then still to be determined whether this intercalation behaviour will be similar with a single-phase material.

To date, more rigorous studies are required to gain further understanding of the Mg^{2+} charge compensation mechanism occurring in the MgMn_2O_4 spinel. To start, reports should provide readers with structural data of the pristine material that includes Mg concentration, Mn oxidation state, inversion degree and spinel:rocksalt ratio. Furthermore, research studies must include electrochemical data obtained from a three-electrode cell to decouple cathode and Mg metal processes, and compelling cathode characterisation data to discriminate (quantitatively) between parasitic electrolytic and intercalation reactions. These characterisation techniques must be able to determine changes in the chemical composition, redox chemistry and structure.³⁸ When possible, operando studies should also be prioritised to better capture real-time battery processes although we acknowledge that these experiments will demand further experiment design, e.g. cell reconstruction to incorporate three electrodes, cell heating elements. This can perhaps explain the current lack of operando studies in the literature.

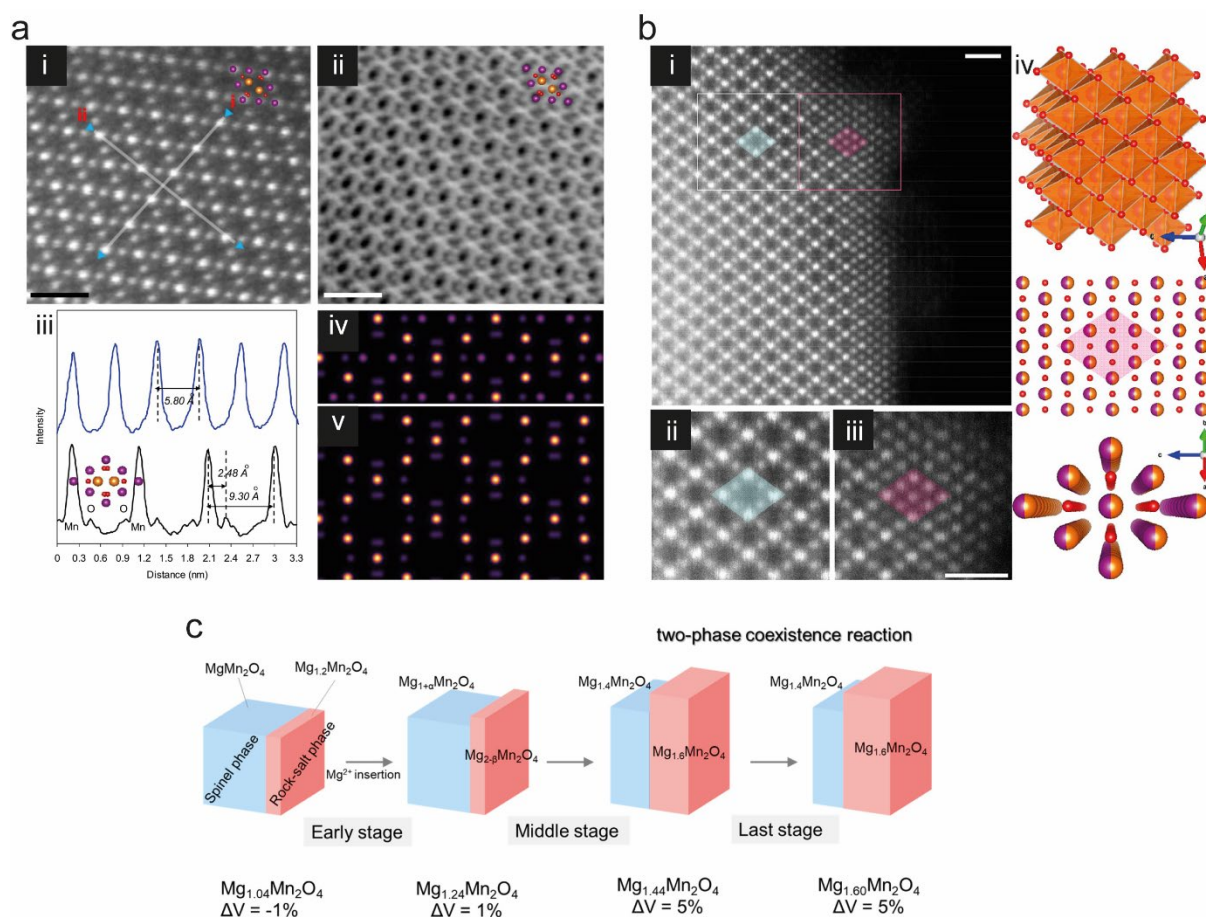


Figure 2 a. STEM characterization of demagnesiated $\text{Mg}_{1-x}\text{Mn}_2\text{O}_4$. (i) HAADF image of $\text{Mg}_{1-x}\text{Mn}_2\text{O}_4$ particle viewed along $[010]$ direction. (ii) ADF image of $\text{Mg}_{1-x}\text{Mn}_2\text{O}_4$ particle viewed along $[010]$ direction. The superimposed atomic arrays on the inset indicate the locations of atom columns. Scale bar, 10 Å. (iii) Intensity line profiles showing the image intensity as a function of position in the HAADF images taken along the highlighted lines in panel a. (iv, v) Simulated ADF micrographic of tetragonal phase MgMn_2O_4 and demagnesiated phase $\text{Mg}_{1-x}\text{Mn}_2\text{O}_4$, respectively viewed at $[010]$ zone axis with ordered Mg vacancies arrangements.^{15, (*)} (Reproduced from ref. 15 with permission from Elsevier, Copyright 2020) **b.** STEM characterization of MgMn_2O_4 surface. (i) HAADF image of MgMn_2O_4 particle viewed along $[110]$ direction with visualization of both the bulk and the surface. (ii, iii) Magnified images shows the spinel phase in the bulk (blue), while a new phase (red diamond) is found at the surface. (iv) Schematic illustrations for the rocksalt MgMn_2O_4 structure viewed along $[110]$ axis. Mg/Mn occupy octahedral sites at the centre of the diamond. Scale bar, 1 nm.³³ (Reproduced from ref. 33 with permission from American Chemical Society, Copyright 2017) **c.** Schematic illustration of the volume changes and phase transition model for the transition from spinel phase to rock-salt phase upon magnesium ion insertion.³⁷ (Reproduced from ref. 37 with permission from American Chemical Society, Copyright 2021)

Effect of electrolyte

Given the extensive choice of liquid electrolyte solutions used when testing the performance of the MgMn_2O_4 spinel, which include aqueous,^{39,40} non-aqueous,^{39,40} and ionic liquid^{14,32} electrolyte media, establishing an accurate comparison in the electrochemical response of MgMn_2O_4 is extremely challenging, especially when these are tested at different temperatures ($\geq 40^\circ\text{C}$) to enhance Mg ion mobility. Indeed, calculated migration barriers have been reported to be as high as 400-800 meV.^{13,14,22}

Electrochemical tests undertaken in aqueous media are performed typically with beaker-type cells with a considerable electrolyte excess⁴⁰⁻⁴², while those carried out in non-aqueous electrolytes and ionic liquids are typically conducted in three-electrode Swagelok⁴⁰ or coin-cell type cells³³. Differences in electrochemical behaviour concerning cell design are being outlined in reference^{27,(*)}, showing that the capacity retention in cubic MgMn_2O_4 increased from $\approx 50\%$ to $\approx 95\%$ from the 2nd to the 10th cycle by replacing an electrochemical beaker-type cell with a coin-cell. Comparative studies amid aqueous and non-aqueous electrolytes have shown that the presence of water improves capacity retention. For instance, Yin et al. showed how the capacity retention could be improved from 30% to 74% by adding 3M H_2O in acetonitrile to 0.5 M $\text{Mg}(\text{TFSI})_2$ in acetonitrile /0.5 M dipropylene glycol dimethyl ether.³⁹ The improvement in specific capacity may be understood by the shielding effect of water molecules with Mg^{2+} ions, facilitating their mobility and hence, its reversible intercalation. It is suggested that water can reduce the Mg^{2+} ion de-solvation energy, facilitating the subtraction of Mg^{2+} ions from the MgMn_2O_4 structure in the charge process.⁴³ However, other reports suggest that water facilitates the dissociation of Mg^{2+} ions from the anionic counterpart of the electrolyte salt (e.g. TFSI^- anions in $\text{Mg}(\text{TFSI})_2$), resulting in more “free” Mg^{2+} ions available in the electrolyte solution.⁴⁴

Another possible explanation for the higher capacity in aqueous electrolytes is proton cycling however, further investigations are required to clarify the observed variabilities in the specific capacity as well as the role of solvent co-intercalation on improving Mg^{2+} ion kinetics and its compatibility with the Mg metal anode. Indeed, while water-containing organic and aqueous electrolytes seem to be an ideal choice compared to non-aqueous systems in terms of cathode performance, these preclude from the use of Mg metal due to the formation of a non-conducting and passivating film on its surface consisting mainly of $\text{Mg}(\text{OH})_2$ and MgO .⁴ Moreover, insulating surface layers are equally formed upon contact between commercial salts and Mg metal, and thus, custom-made salts are generally required, where weakly coordinating anions are desired (e.g. $\text{Mg}(\text{PF}_6)_2(\text{CH}_3\text{CN})_6$).⁴⁵ Their synthesis is nonetheless complicated, hindering their commercial application. A reversible cell containing Mg metal would be possible if the anode can be protected effectively from SEI formation while allowing

stable Mg deposition and dissolution, for example, with the growth of an ion-conducting artificial SEI layer⁴⁶. Alternatively, Mg metal can be substituted by other anode materials, such as V_2O_5 ,⁴⁰ carbon,^{33,34} and Pt mesh⁴⁷ which should be compatible with the aqueous electrolytes. To the best of our knowledge, the best capacity results for the first discharge (in a non-aqueous electrolyte) were reported by Truong et al., showing a capacity of 170 mAh g^{-1} (at a current density of 3.8 mA g^{-1}) using active carbon as the anode in a coin cell. The capacity was obtained through the reversible oxidation of Mn(III) to Mn(IV) at $\sim 3.0 \text{ V vs. Mg}^{2+}/\text{Mg}$. For the aqueous electrolyte counterpart, one of the most promising results was achieved by Liu et al who show a reversible discharge capacity of 80 mA h g^{-1} at a high current rate (1000 mA g^{-1}) around 0.1 V vs. SHE ($\sim 2.3 \text{ V vs. Mg}^{2+}/\text{Mg}$) in a beaker-type cell.⁴¹

In conclusion, moving forward, it is more than evident the urgency to establish standard measuring and experimental protocols among the research community. These should consider at least, reaction temperature and type of cell, electrode reference and electrolyte (and its water content). Ideally, to facilitate comparisons among groups, reaction temperature needs to be kept as close as possible to room temperature operation to minimise side reactions within the cathode (e.g. metal migration) and electrolyte material (e.g. salt decomposition, solvent evaporation) and at their interface. Furthermore, electrochemical tests need to be undertaken with three-electrode cells that can exert good contact between working and counter electrode, a stable reference such as glassy carbon, and where possible, with widely accessible off-the-shelf electrolyte salts and solvents to allow for good data comparison. Water in electrolytes is to be kept minimal to discard proton contribution to the Mg^{2+} intercalation processes occurring in these materials, raising the need to establish electrolyte drying protocols. Yet, a consensus about the aforementioned conditions across different research groups remains unachieved most likely due to the lack of systematic studies available to inform on best practices to the research community. We expect however that as the field advances and the amount of literature in this area increases this problem will be solved.

Effect of crystallite engineering and surface modification

Particle size and morphology have been shown to play a key role in the electrochemical properties of MgMn_2O_4 . Canepa et al. demonstrated the strong interdependence between particle size and migration barriers for multivalent ions using computational methods.⁴⁸ Reducing Mg^{2+} ion migration barriers through crystallite size and morphology modification enhances the storage of Mg^{2+} ions in MgMn_2O_4 by decreasing the voltage hysteresis. Furthermore, large surface areas increase the overall capacity of the cathode, by increasing the pseudocapacitive contribution to the specific capacity. For example, Doi et al. compared the electrochemical behaviour of dense MgMn_2O_4 nanoparticle aggregates with that of

nanoplates with a width of ~ 100 nm and a thickness of ~ 14 nm (**Figure 3a**).^{31,(*)} Nanoplates showed a reduced overpotential compared to nanoparticles, allowing for higher demagnesiated states (i.e. higher capacity values) before reaching the potential at which electrolyte degradation occurred (**Figure 3b**). Furthermore, Yin et al. reported a 3-fold increase in specific capacity using a non-aqueous electrolyte when decreasing the crystallite size from 31 to 11 nm in MgMn_2O_4 nanoparticles synthesized by the Pechini method.³⁹ Nevertheless, a higher surface-to-bulk ratio may result in lower capacity retention values since structural changes such as the spinel-to-rock-salt phase transition occurring at high levels of demagnesiatioin in the material tend to occur at the oxygen-deficient particle surface.³³ This may explain the lower capacity retention after 40 cycles observed in the 11 nm nanoparticles (28%) compared to that of the 31 nm nanoparticles (58%).³⁹ Similarly, surface modification strategies including carbon composite fabrication⁴¹, and coatings, e.g. V_2O_5 ,^{31,49} have shown to improve the interfacial properties of MgMn_2O_4 by promoting Mg^{2+} diffusion and charge-transfer reactions and suppressing undesirable reactions with the electrolyte.

It is expected that in the coming years there will be a growing number of works that consider nanosized and/or surface-modified spinel cathodes to enhance Mg^{2+} ion mobility and unlock the storage capability in spinel materials. From a fundamental understanding point of view, these strategies will be helpful to truly determine the maximal degree of Mg^{2+} ion extraction/insertion in MgMn_2O_4 . Nano sizing, however, will undoubtedly compromise the cycle-life and Coulombic efficiency of these materials due to an increase of surface reactions (spinel-rocksalt transition) and at the cathode-electrolyte interface. Therefore, this approach will most likely reinforce the need for electrolytes compatible with high-voltage cathodes, triggering further Mg-based electrolyte research. In the meantime, it is best to consider nanosizing strategies in conjunction with the use of surface coatings to reduce secondary reactions with the electrolyte given the larger surface area of the nanomaterial. In turn, this area of research should benefit from previous know-how in coating technologies and materials used in most well-known technologies such as Li-ion batteries.

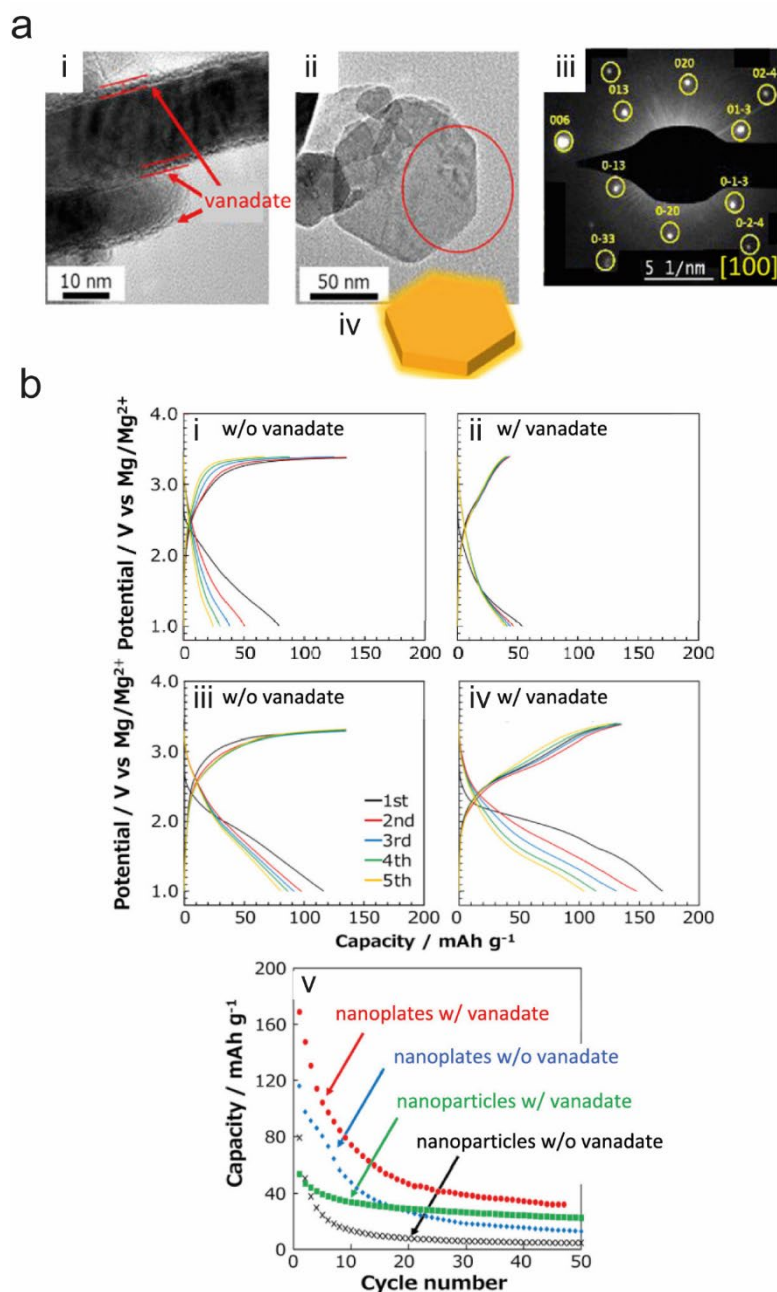


Figure 3 a. TEM images (side view (i) and plan view (ii)), SAED pattern (iii), and schematic illustration (iv) of MgMn_2O_4 nanoplating coated with vanadate by the conventional drying process in air. The SAED pattern (iii) was obtained from the area denoted by a red circle in (ii). **b.** Discharge/charge curves at 100 °C of MgMn_2O_4 nanoparticles without (i) and with vanadate (ii) and MgMn_2O_4 nanoplating without (iii) and with vanadate (iv) at 1/10 C. The thinner vanadate layer was produced by the freeze-drying process. Cyclability curves at 100 °C of MgMn_2O_4 nanoplating with and without vanadate and nanoparticles with and without vanadate at 1/10 C (v)³¹. (Reproduced from ref. 31 with permission from American Chemical Society, Copyright 2020)

Effect of TM substitution and vacancies

3d transition metal substitution and (co)substitution strategies using Ti,⁵⁰ Cr,^{23,(*)} Fe,^{51,52} Co,⁵³ and Ni⁵⁴ to replace Mn³⁺ ions in MgMn₂O₄ have been explored to enhance the electrochemical performance of MgMn₂O₄.

To date, very promising results have been reported by Kwon et al. on the MgCrMnO₄ spinel in a non-aqueous electrolyte showing reversible bulk Mg²⁺ (de)intercalation at moderately high potentials, achieving an energy density upon the first discharge which corresponds to 180 Wh Kg⁻¹ (at 60 °C) (**Figure 4a**).^{23,(*)} MgCrMnO₄ combines the advantages of high Mg²⁺ mobility in the MgCr₂O₄ spinel parent material due to the presence of Mg²⁺-Cr³⁺ bonds^{55,56}, and thus, reduced extraction/insertion overpotential, and a suitable high redox potential arising from the Mg²⁺-Mn³⁺ bonds. Furthermore, reports on Mg(Mn_{1-x}Fe_x)₂O₄ spinels have shown Fe ions to be catalytically less active than Mn ions in the oxidative decomposition of the 0.3 M [Mg(tetraglyme)][TFSA]₂ in bis(tri-fluoromethylsulfonyl)amide electrolytic solution and aqueous electrolytes, showing enhanced cycling stability in spinel compositions with high Fe:Mn ratios (**Figure 4b**).^{51,52} More recently, Medina et al. have reported on the benefits of creating Mn and Mg defective spinels (Mg_xMn_{2-y}O_{4-z}) to decrease the percolation energy of Mg²⁺ ions in the spinel framework structure, using a bond valence energy approach.^{36,(**)} These results backed up their experimental data showing small charge-discharge polarisation in a Mg_{0.3}Mn_{2-y}O₄ sample (compared to stoichiometric MgMn₂O₄) (**Figure 4c**).

Materials design development by substitution of Jahn-Teller active Mn³⁺ ions with other elements is *a priori* beneficial to avoid strain effects at the phase boundary between the spinel and rocksalt phases upon Mg extraction. However, several considerations need to be made in advance to truly understand the benefits of this strategy. For example, attention must be paid to the chemical stability of the rocksalt phases formed as some of these have been reported to disproportionate in ambient conditions.¹⁴ Furthermore, certain elemental substitutions using high-voltage redox couples may increase the average reaction potential of the spinel cathode and thus, its energy density. One must carefully consider this point since the substituent redox chemistry might occur above the stability voltage windows of the electrolyte and thus, it can significantly reduce the Mg storage capability of the spinel material. For example, in the Cr-Mn and Fe-Mn works cited above, Mn ions were reported to be the only redox-active species responsible for the observed charge/discharge capacities. This illustrates, once again, the cathode-electrolyte interdependency and thus, efforts must come from both research disciplines to make significant research progress. From a fundamental point of view, this area is still in its infancy, most likely due to still unresolved questions with the more simplistic MgMn₂O₄ system. Thus, it is unquestionable that in the future there will be more works devoted to the understanding of the structural role of the dopants in the spinel

material, e.g. will different dopants adopt distinctive preferential crystal sites?, and more in-depth studies related to their effects on the electrochemical performance, e.g. do these segregate to the surface during cycling; to which extent they help reducing inversion (if they do)?

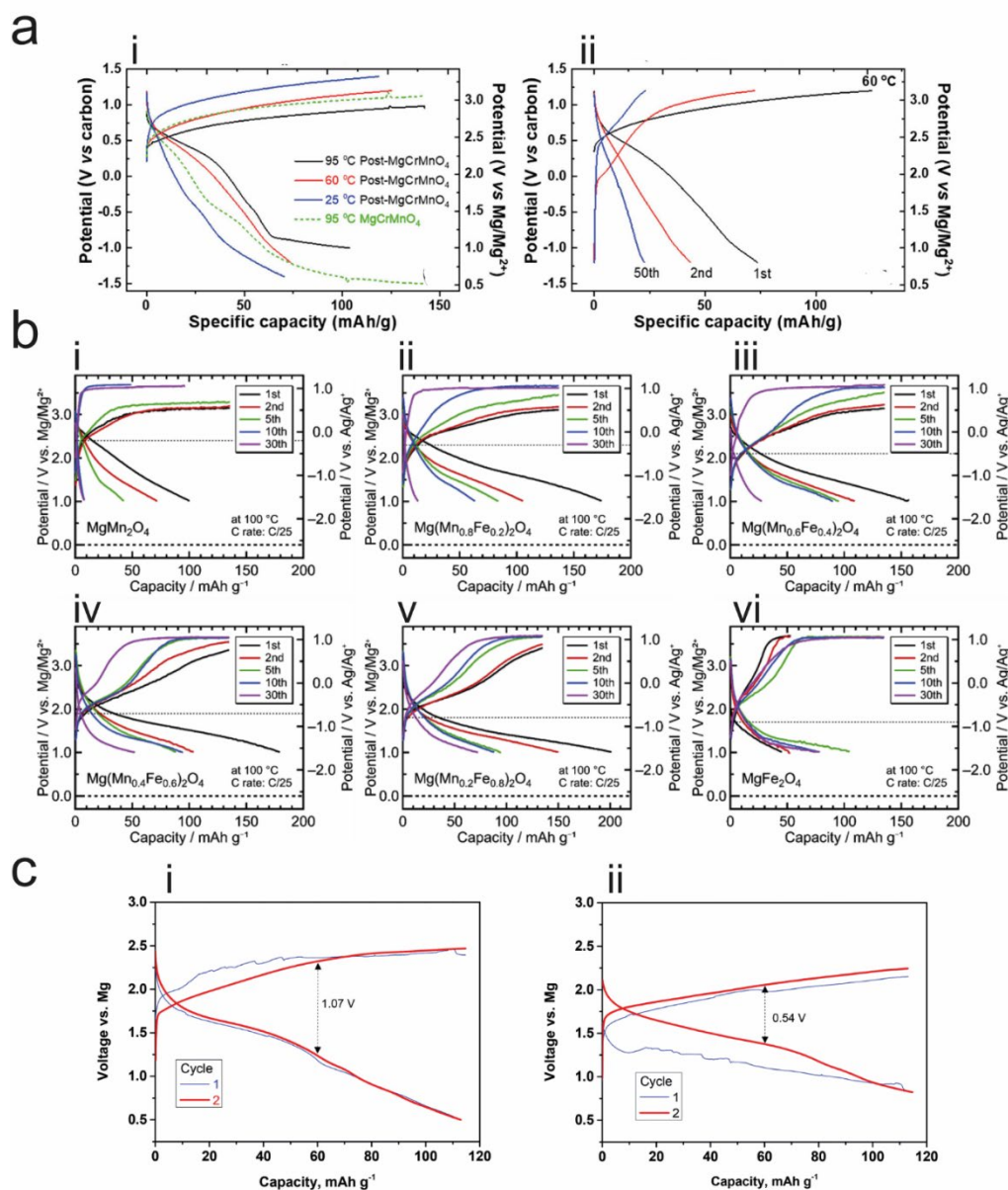


Figure 4 i. Representative potential versus capacity profiles of post-MgCrMnO₄ (solid line) and MgCrMnO₄ (dash line) at (c) variable temperatures and (d) the different number of cycles at 60 °C when paired with a carbon counter electrode.^{23,(*)} (Reproduced from ref. 23 with permission from American Chemical Society, Copyright 2020) **ii.** Cyclic voltammograms of Mg(Mn_{1-x}Fe_x)₂O₄ synthesized at 500 °C for 24 h: (a) x = 0, (b) 0.2, (c) 0.4, (d) 0.6, (e) 0.8, (f) 1 in 0.3 M [Mg(G4)][TFSA]₂/P13TFSA measured at 100 °C. CE: Mg ribbon, RE: Ag wire in G3

containing 0.01 M AgNO₃ and 0.10 M Mg(TFSA)₂. Scan rate was 25 μV s⁻¹.⁵¹ (Reproduced from ref. 51 with permission from Elsevier, Copyright 2019) **iii.** Voltage curves for MgMn₂O₄ in the Mg cell before (a) and after acid-treatment (b). Electrolyte: Mg(TFSI)₂ in DME. Current density: 5 mA g⁻¹.^{36, (**)} (Reproduced from ref. 36 with permission from The Royal Society of Chemistry, Copyright 2021)

Concluding Remarks

Despite the enormous potential of oxyspinels as high-voltage cathode materials for RMBs, there are remaining challenges at a fundamental level of understanding on the baseline MgMn₂O₄ material which are an obstacle to realizing their full potential in RMBs. To date, fundamental knowledge in this area is mainly based on computational studies which require further experimental validation. In turn, experimental validation demands standardized protocols across different studies. For instance, reports must include the inversion degree in MgMn₂O₄ and a quantitative elemental determination to ascertain the degree of Jahn-Teller distortion and redox available species. This will allow a better insight into the structure-property relationship in these materials when tested in RMBs. Moreover, the electrochemical testing of MgMn₂O₄ comes with its challenges, including high Mg migration barriers and incompatibility with Mg and some electrolytic solutions, driving researchers into system modifications which include but are not limited to increasing testing temperatures, Mg surface protection, use of more stable anodes and electrolyte additives. Altogether, these approaches preclude from drawing accurate comparisons between published systems. Last, some open questions which still require further understanding are the extent of Mg intercalation within the structure, and the role of Mn/Mg antisite defects and H⁺ (either attained from solvent decomposition or water impurities in the electrolyte) in the intercalation process. This research will necessitate the use of combined advanced techniques preferably under operando or in-situ conditions at varied length scales to fully interrogate these battery systems. We believe that full realization of this knowledge, together with advances in high-voltage electrolyte research, must be achieved to advance into more innovative sister compounds with enhanced Mg-ion mobility such as the recently discovered Cr-based oxyspinels or more complex systems involving hybrid spinel compounds containing oxygen and softer anions such as S or Se.

Conflict of interest statement

The authors declare that they have no conflicts of interest

Acknowledgements

The authors gratefully acknowledge Lancaster University for the provision of a PhD scholarship to Alexandra Michail.

References

1. Durmus, Y. E., Zhang, H., Baakes, F., Desmaizieres, G., Hayun, H., Yang, L., Kolek, M., Küpers, V., Janek, J., Mandler, D., Passerini, S. & Ein-Eli, Y. Side by Side Battery Technologies with Lithium-Ion Based Batteries. *Adv. Energy Mater.* **10**, 2000089 (2020).
2. Liang, Y., Dong, H., Aurbach, D. & Yao, Y. Current status and future directions of multivalent metal-ion batteries. *Nature Energy* 1–11 (2020) doi:10.1038/s41560-020-0655-0.
3. Kim, H., Jeong, G., Kim, Y. U., Kim, J. H., Park, C. M. & Sohn, H. J. Metallic anodes for next generation secondary batteries. *Chemical Society Reviews* vol. 42 9011–9034 (2013).
4. Lu, Z., Schechter, A., Moshkovich, M. & Aurbach, D. On the electrochemical behavior of magnesium electrodes in polar aprotic electrolyte solutions. *J. Electroanal. Chem.* **466**, 203–217 (1999).
5. Zhang, J., Yao, X., Misra, R. K., Cai, Q. & Zhao, Y. Progress in electrolytes for beyond-lithium-ion batteries. *J. Mater. Sci. Technol.* **44**, 237–257 (2020).
6. Shuai, H., Xu, J. & Huang, K. Progress in retrospect of electrolytes for secondary magnesium batteries. *Coordination Chemistry Reviews* vol. 422 213478 (2020).
7. Ling, C. & Zhang, R. *Manganese dioxide as rechargeable magnesium battery cathode*. *Frontiers in Energy Research* vol. 5 30 (Frontiers Media S.A., 2017).
8. Zhang, Y., Geng, H., Wei, W., Ma, J., Chen, L. & Li, C. C. Challenges and recent progress in the design of advanced electrode materials for rechargeable Mg batteries. *Energy Storage Mater.* **20**, 118–138 (2019).
9. Pei, C., Xiong, F., Yin, Y., Liu, Z., Tang, H., Sun, R., An, Q. & Mai, L. Recent Progress and Challenges in the Optimization of Electrode Materials for Rechargeable Magnesium Batteries. *Small* **17**, 2004108.
10. Mao, M., Gao, T., Hou, S. & Wang, C. A critical review of cathodes for rechargeable Mg batteries. *Chem. Soc. Rev.* **47**, 8804–8841 (2018).
11. Levi, E., YGofar & Aurbach, D. On the way to rechargeable Mg batteries: The challenge of new cathode materials. *Chem. Mater.* **22**, 860–868 (2010).

12. Kim, C., Phillips, P. J., Key, B., Yi, T., Nordlund, D., Yu, Y.-S. S., Bayliss, R. D., Han, S.-D. D., He, M., Zhang, Z., Burrell, A. K., Klie, R. F. & Cabana, J. Direct Observation of Reversible Magnesium Ion Intercalation into a Spinel Oxide Host. *Adv. Mater.* **27**, 3377–3384 (2015).
13. Liu, M., Rong, Z., Malik, R., Canepa, P., Jain, A., Ceder, G. & Persson, K. A. Spinel compounds as multivalent battery cathodes: A systematic evaluation based on ab initio calculations. *Energy Environ. Sci.* **8**, 964–974 (2015).
14. Okamoto, S., Ichitsubo, T., Kawaguchi, T., Kumagai, Y., Oba, F., Yagi, S., Shimokawa, K., Goto, N., Doi, T. & Matsubara, E. Intercalation and Push-Out Process with Spinel-to-Rocksalt Transition on Mg Insertion into Spinel Oxides in Magnesium Batteries. *Adv. Sci.* **2**, 1500072 (2015).
15. Truong, Q. D., Kobayashi, H., Nayuki, K., Sasaki, Y. & Honma, I. Atomic-scale observation of phase transition of MgMn₂O₄ cubic spinel upon the charging in Mg-ion battery. *Solid State Ionics* **344**, 115136 (2020).
16. Kolli, S. K. & Van Der Ven, A. Controlling the Electrochemical Properties of Spinel Intercalation Compounds. *ACS Appl. Energy Mater.* **1**, 6833–6839 (2018).
17. Irani, K. S., Sinha, A. P. B. & Biswas, A. B. Crystal distortion in spinels containing Mn³⁺ ions. *J. Phys. Chem. Solids* **17**, 101–111 (1960).
18. Reed, J. & Ceder, G. Role of electronic structure in the susceptibility of metastable transition-metal oxide structures to transformation. *Chem. Rev.* **104**, 4513–4533 (2004).
19. Radhakrishnan, N. K. & Biswas, A. B. A neutron diffraction study of the cation migration in MgMn₂O₄. *Phys. Status Solidi* **37**, 719–722 (1976).
20. Rosenberg, M. & Nicolau, P. Electrical Properties and Cation Migration in MgMn₂O₄. *Phys. status solidi* **6**, 101–110 (1964).
21. Malavasi, L., Ghigna, P., Chiodelli, G., Maggi, G. & Flor, G. Structural and Transport Properties of Mg_{1-x}Mn_xMn₂O_{4±δ} Spinel. *J. Solid State Chem.* **166**, 171–176 (2002).
22. Sai Gautam, G., Canepa, P., Urban, A., Bo, S.-H. & Ceder, G. Influence of Inversion on Mg Mobility and Electrochemistry in Spinel. *Chem. Mater.* **29**, 7918–7930 (2017).
23. Kwon, B. J., Yin, L., Park, H., Parajuli, P., Kumar, K., Kim, S., Yang, M., Murphy, M., Zapol, P., Liao, C., Fister, T. T., Klie, R. F., Cabana, J., Vaughey, J. T., Lapidus, S. H.

- & Key, B. High Voltage Mg-Ion Battery Cathode via a Solid Solution Cr–Mn Spinel Oxide. *Chem. Mater.* **32**, 6577–6587 (2020).
24. Mănăilă, R. & Păușescu, P. Structural Changes in MgMn_2O_4 at High Temperatures. *Phys. status solidi* **9**, 385–394 (1965).
 25. Malavasi, L., Tealdi, C., Flor, G. & Amboage, M. High-pressure stability of the tetragonal spinel MgMn_2O_4 : Role of inversion. *Phys. Rev. B - Condens. Matter Mater. Phys.* **71**, 174102 (2005).
 26. Feng, Z., Chen, X., Qiao, L., Lipson, A. L., Fister, T. T., Zeng, L., Kim, C., Yi, T., Sa, N., Proffit, D. L., Burrell, A. K., Cabana, J., Ingram, B. J., Biegalski, M. D., Bedzyk, M. J. & Fenter, P. Phase-Controlled Electrochemical Activity of Epitaxial Mg-Spinel Thin Films. *ACS Appl. Mater. Interfaces* **7**, 28438–28443 (2015).
 27. Kobayashi, H., Yamaguchi, K. & Honma, I. Rapid room-Temperature synthesis of ultrasmall cubic Mg-Mn spinel cathode materials for rechargeable Mg-ion batteries. *RSC Adv.* **9**, 36434–36439 (2019).
 28. Paris, E., Ross II, C. R. & Olijnyk, H. Mn_3O_4 at high pressure: a diamond-anvil cell study and a structural modelling. *Eur. J. Mineral.* **4**, 87–94 (1992).
 29. Malavasi, L., Tealdi, C., Amboage, M., Mozzati, M. C. & Flor, G. High pressure X-ray diffraction study of MgMn_2O_4 tetragonal spinel. in *Nuclear Instruments and Methods in Physics Research, Section B: Beam Interactions with Materials and Atoms* vol. 238 171–174 (North-Holland, 2005).
 30. Ling, C. & Mizuno, F. Phase Stability of Post-spinel Compound AMn_2O_4 (A = Li, Na, or Mg) and Its Application as a Rechargeable Battery Cathode. *Chem. Mater.* **25**, 3062–3071 (2013).
 31. Doi, S., Ise, R., Mandai, T., Oaki, Y., Yagi, S. & Imai, H. Spinel-Type MgMn_2O_4 Nanoplates with Vanadate Coating for a Positive Electrode of Magnesium Rechargeable Batteries. *Langmuir* **36**, 8537–8542 (2020).
 32. Hatakeyama, T., Okamoto, N. L., Shimokawa, K., Li, H., Nakao, A., Uchimoto, Y., Tanimura, H., Kawaguchi, T. & Ichitsubo, T. Electrochemical phase transformation accompanied with Mg extraction and insertion in a spinel MgMn_2O_4 cathode material. *Phys. Chem. Chem. Phys.* **21**, 23749–23757 (2019).
 33. Truong, Q. D., Kempaiah Devaraju, M., Tran, P. D., Gambe, Y., Nayuki, K., Sasaki, Y. & Honma, I. Unravelling the Surface Structure of MgMn_2O_4 Cathode Materials for

- Rechargeable Magnesium-Ion Battery. *Chem. Mater.* **29**, 6245–6251 (2017).
34. Shimokawa, K. & Ichitsubo, T. Spinel–rocksalt transition as a key cathode reaction toward high-energy-density magnesium rechargeable batteries. *Current Opinion in Electrochemistry* vol. 21 93–99 (2020).
 35. Tang, D., Sun, Y., Yang, Z., Ben, L., Gu, L. & Huang, X. Surface structure evolution of LiMn₂O₄ cathode material upon charge/discharge. *Chem. Mater.* **26**, 3535–3543 (2014).
 36. Medina, A., Rodríguez, A. I., Pérez-Vicente, C. & Alcántara, R. Testing the reversible insertion of magnesium in a cation-deficient manganese oxy-spinel through a concentration cell. *Dalt. Trans.* **50**, 2123–2130 (2021).
 37. Tuerxun, F., Otani, S., Yamamoto, K., Matsunaga, T., Imai, H., Mandai, T., Watanabe, T., Uchiyama, T., Kanamura, K. & Uchimoto, Y. Phase Transition Behavior of MgMn₂O₄ Spinel Oxide Cathode during Magnesium Ion Insertion. *Chem. Mater.* **33**, 1006–1012 (2021).
 38. Johnson, I. D., Ingram, B. J. & Cabana, J. The Quest for Functional Oxide Cathodes for Magnesium Batteries: A Critical Perspective. *ACS Energy Lett.* 1892–1900 (2021) doi:10.1021/acsenergylett.1c00416.
 39. Yin, J., Brady, A. B., Takeuchi, E. S., Marschilok, A. C. & Takeuchi, K. J. Magnesium-ion battery-relevant electrochemistry of MgMn₂O₄: crystallite size effects and the notable role of electrolyte water content. *Chem. Commun.* **53**, 3665–3668 (2017).
 40. Cabello, M., Alcántara, R., Nacimiento, F., Ortiz, G., Lavela, P. & Tirado, J. L. Electrochemical and chemical insertion/deinsertion of magnesium in spinel-type MgMn₂O₄ and lambda-MnO₂ for both aqueous and non-aqueous magnesium-ion batteries. *CrystEngComm* **17**, 8728–8735 (2015).
 41. Liu, G., Chi, Q., Zhang, Y., Chen, Q., Zhang, C., Zhu, K. & Cao, D. Superior high rate capability of MgMn₂O₄/rGO nanocomposites as cathode materials for aqueous rechargeable magnesium ion batteries. *Chem. Commun.* **54**, 9474–9477 (2018).
 42. Zhang, D., Chen, Q., Zhang, J. & Sun, T. MgMn₂O₄/multiwalled carbon nanotubes composite fabricated by electrochemical conversion as a high-performance cathode material for aqueous rechargeable magnesium ion battery. *J. Alloys Compd.* **873**, 159872 (2021).
 43. Nam, K. W., Kim, S., Lee, S. S. S., Salama, M., Shterenberg, I., Gofer, Y., Kim, J. S.

- J. S., Yang, E., Park, C. S., Kim, J. S. J. S., Lee, S. S. S., Chang, W. S., Doo, S. G., Jo, Y. N., Jung, Y., Aurbach, D. & Choi, J. W. The High Performance of Crystal Water Containing Manganese Birnessite Cathodes for Magnesium Batteries. *Nano Lett.* **15**, 4071–4079 (2015).
44. Johnston, B., Henry, H., Kim, N. & Lee, S. B. Mechanisms of Water-Stimulated Mg²⁺ Intercalation in Vanadium Oxide: Toward the Development of Hydrated Vanadium Oxide Cathodes for Mg Batteries. *Front. Energy Res.* **8**, 361 (2021).
 45. Keyzer, E. N., Glass, H. F. J., Liu, Z., Bayley, P. M., Dutton, S. E., Grey, C. P. & Wright, D. S. Mg(PF₆)₂-Based Electrolyte Systems: Understanding Electrolyte-Electrode Interactions for the Development of Mg-Ion Batteries. *J. Am. Chem. Soc.* **138**, 8682–8685 (2016).
 46. Son, S. B., Gao, T., Harvey, S. P., Steirer, K. X., Stokes, A., Norman, A., Wang, C., Cresce, A., Xu, K. & Ban, C. An artificial interphase enables reversible magnesium chemistry in carbonate electrolytes. *Nat. Chem.* **10**, 532–539 (2018).
 47. Sun, X., Duffort, V., Mehdi, B. L., Browning, N. D. & Nazar, L. F. Investigation of the Mechanism of Mg Insertion in Birnessite in Nonaqueous and Aqueous Rechargeable Mg-Ion Batteries. *Chem. Mater.* **28**, 534–542 (2016).
 48. Canepa, P., Sai Gautam, G., Hannah, D. C., Malik, R., Liu, M., Gallagher, K. G., Persson, K. A. & Ceder, G. Odyssey of Multivalent Cathode Materials: Open Questions and Future Challenges. *Chem. Rev.* **117**, 4287–4341 (2017).
 49. Ishii, K., Doi, S., Ise, R., Mandai, T., Oaki, Y., Yagi, S. & Imai, H. Structured spinel oxide positive electrodes of magnesium rechargeable batteries: High rate performance and high cyclability by interconnected bimodal pores and vanadium oxide coating. *J. Alloys Compd.* **816**, 152556 (2020).
 50. Zainol, N. H., Hambali, D., Osman, Z., Kamarulzaman, N. & Rusdi, R. Synthesis and characterization of Ti-doped MgMn₂O₄ cathode material for magnesium ion batteries. *Ionics (Kiel)*. **25**, 133–139 (2019).
 51. Han, J., Yagi, S. & Ichitsubo, T. Suppressive effect of Fe cations in Mg(Mn_{1-x}Fe_x)₂O₄ positive electrodes on oxidative electrolyte decomposition for Mg rechargeable batteries. *J. Power Sources* **435**, 226822 (2019).
 52. Zhang, Y. Y., Liu, G., Zhang, C., Chi, Q., Zhang, T., Feng, Y., Zhu, K., Zhang, Y. Y., Chen, Q. & Cao, D. Low-cost MgFe_xMn_{2-x}O₄ cathode materials for high-performance aqueous rechargeable magnesium-ion batteries. *Chem. Eng. J.* **392**, 123652 (2020).

53. Banu, A., A.Sakunthala, Thamilselvan, M., Kumar, P. S., Suresh, K. & Ashwini, S. Preparation, characterization and comparative electrochemical studies of MgMXMn₂XO₄ (x=0, 0.5; M= Ni/Co). *Ceram. Int.* **45**, 13072–13085 (2019).
54. Jin, W., Yin, G., Wang, Z. & Fu, Y. Q. Surface stability of spinel MgNi_{0.5}Mn_{1.5}O₄ and MgMn₂O₄ as cathode materials for magnesium ion batteries. *Appl. Surf. Sci.* **385**, 72–79 (2016).
55. Bayliss, R. D., Key, B., Sai Gautam, G., Canepa, P., Kwon, B. J., Lapidus, S. H., Dogan, F., Adil, A. A., Lipton, A. S., Baker, P. J., Ceder, G., Vaughey, J. T. & Cabana, J. Probing Mg Migration in Spinel Oxides. *Chem. Mater.* **32**, 663–670 (2020).
56. Chen, T., Sai Gautam, G., Huang, W. & Ceder, G. First-Principles Study of the Voltage Profile and Mobility of Mg Intercalation in a Chromium Oxide Spinel. *Chem. Mater.* **30**, 153–162 (2018).